

Development of a bias power supply for Geiger mode avalanche photodiodes*

MENG Yinjie^{1,2}, WEI Zhengjun^{1,2**}, YAN Ziling^{1,2}, and WANG Jindong¹

1. Guangdong Provincial Key Laboratory of Quantum Engineering and Quantum Materials, South China Normal University, Guangzhou 510006, China

2. Guangdong Provincial Key Laboratory of Nanophotonic Functional Materials and Devices, South China Normal University, Guangzhou 510006, China

(Received 3 April 2023; Revised 28 May 2023)

©Tianjin University of Technology 2023

Avalanche photodiodes (APDs) have high output and high stability requirements for bias power in Geiger mode. This paper designs an APD with high boost ratio, high precision, low temperature drift, small size, and low power. Bias power supply, this module uses switching chip IC and flyback transformer to achieve high step-up ratio, realizes precise output control through precision operational amplifier and T-type resistor feedback network, and designs appropriate compensation network to improve system stability. The size of the module is 2.5 cm×2.5 cm, the output voltage is adjustable from 0 to 450 V, and the maximum ripple does not exceed 5.4 mV. By changing the control voltage, any type of APD in Geiger mode can be biased, and the maximum deviation of the bias voltage does not exceed 0.5%.

Document code: A **Article ID:** 1673-1905(2023)11-0659-7

DOI <https://doi.org/10.1007/s11801-023-3057-2>

With the continuous development of communication and detection technology, the detection of weak to single-photon level signals has become an urgent need. The avalanche photodiode (APD) is the key device to realize single photon detection because of its advantages of high responsivity, high quantum efficiency, fast response speed, less susceptible to magnetic field interference and easy integration, and is widely used in laser ranging, quantum key distribution, fluorescence lifetime detection, biomedical and optical fiber communication and other fields^[1-5]. According to the APD gain characteristics, it is necessary to give the APD a reverse bias voltage higher than its avalanche breakdown voltage, so that it is in Geiger mode, and the internal avalanche breakdown effect is used to achieve high gain, and realize the weak signal at the single photon level probing^[6,7]. When the APD is in Geiger mode, a small change in the reverse bias voltage may cause a great change in the gain of the APD, and some APDs have an avalanche breakdown voltage as high as several hundred volts^[8], which requires the power module not only to realize high voltage output also needs to meet high stability^[9]. At the same time, some emerging application scenarios, such as handheld laser range finders, spaceborne laser detectors and lidar, have put forward requirements for small size and low power for power modules.

Commonly used APD bias power supply schemes in-

clude multi-stage voltage boosting scheme, high frequency transformer scheme and switching power supply scheme. In 2011, WEI et al^[10] used a voltage doubling scheme to achieve a highly stable APD bias power supply, with the highest output voltage of only 45 V and a voltage ripple of 100 μ V. While it meets the requirement for high stability, it cannot meet the needs of high bias voltage applications. Furthermore, the power supply has a large volume due to the multiple filtering components. If a high voltage output is required, many voltage doubling circuits are needed, which could result in a large number of components and a larger system volume. Additionally, the noise is amplified by multiple stages, affecting the output voltage precision. In 2013, YANG et al^[11] used an integrated boost topology switching power supply, with the highest output voltage of 80 V and output ripple of 2.12 mV. Although this power supply system is small in size, the highest output voltage of 80 V still cannot meet the bias needs of APDs with high avalanche breakdown voltages. In 2018, XING et al^[12] designed a bias power supply for silicon APDs using a switching power supply, which could achieve a maximum voltage output of 300 V with a ripple of 20.4 mV. However, the volume of this bias voltage module is relatively large and does not meet the requirements for small size. In 2021, XIANG et al^[13] used a high-frequency transformer method, directly boosting the voltage using

* This work has been supported by the National Nature Science Foundation of China (Nos.62071186 and 61771205), and the Guangdong Provincial Key Laboratory (No.2020B1212060066).

** E-mail: weizhengjun@m.scnu.edu.cn

an oscillation circuit and a high-turns ratio transformer. The power supply module can output a maximum direct-current (DC) voltage of 372 V with a ripple of 12.7 mV and has a small size. Although this high-frequency transformer scheme has a high output voltage and small size, adjusting the output voltage is difficult because the transformer winding ratio is fixed. In addition, the turn ratio of the transformer is high, and to reduce size, the wire diameter of the transformer coil winding is thinner, which causes significant loss and leads to a large deviation between the output voltage and theoretical value.

This paper uses a switching power supply scheme to design a high-precision, high stability, and small volume APD bias power supply. We use an integrated switching power supply chip LT8580 combined with a flyback transformer to achieve high voltage output and reduce the number of components and volume. We focus on improving the feedback control loop, using a T-type resistor feedback network as the feedback resistor to avoid the adverse effects of high resistance feedback resistors in traditional schemes, improving the output voltage stability. We also use precision operational amplifiers as error amplifiers to achieve high precision output voltage. At the same time, we calculate the circuit transfer function, compensate for the loop, improve the stability of the power supply system, and provide a good response speed. The bias power supply designed in this paper can output up to 450 V, adjustable within 0—450 V, with a high precision of 0.5% and a ripple of only 5.4 mV. In addition, the power supply has a volume of only 2.5 cm×2.5 cm. The system is shown in Fig.1, mainly divided into the main circuit and control circuit.

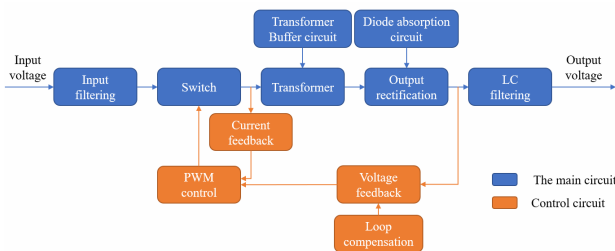


Fig.1 Block diagram of APD bias power supply system

The flyback converter^[14,15] is selected as the main topology circuit of this scheme, because the transformer in the flyback converter is not only a transformer, but also plays an energy storage role, reducing the additional energy storage inductance and reducing the number of components, which can effectively control volume. The schematic diagram is shown in Fig.2. The working principle is as follows. When the switch tube is closed, the input voltage is applied to the primary coil L_p , and L_p stores energy at this time. While the secondary coil L_s and the primary coil L_p have the opposite end, the induced voltage of L_s is negative at the top and positive at

the bottom, and the output diode VD is cut off, the output capacitor C provides energy for the load. When the switch is turned off, the primary inductance L_p transfers energy to the secondary inductance L_s , at this time the voltage on L_s is reversed, the upper positive and the lower negative, the diode VD is turned on, and L_s provides energy for the load energy, and charge the capacitor C, and finally a smooth output DC voltage can be obtained^[16].

Some APDs have an avalanche breakdown voltage as high as several hundred volts, and the maximum reverse bias current in Geiger mode does not exceed 1 mA, so the bias power supply is suitable for working in discontinuous conduction mode (DCM) to avoid output instability^[17,18]. The relationship between the turn ratio and the maximum stress of the switch tube is

$$V_{ms} = V_{in} + N_p/N_s (V_o + 1). \quad (1)$$

In this paper, the input of the power supply V_{in} is 5 V, and the output V_{out} is 450 V. The withstand voltage value of the switch tube is 65 V, and a margin of 30% is reserved. Assuming that the conduction voltage drop of the diode is 1 V, the turn ratio of the transformer N_p/N_s can be obtained as 1/10.

The primary inductance of the transformer can be calculated as

$$L_p = \frac{V_{RF} \times D_{max}}{2P_{in} f_s K_{RF}}. \quad (2)$$

In the DCM mode, the maximum duty cycle D_{max} is 0.45, K_{RF} is 1, and the input power P_{in} is 1 W. In order to reduce the size of the transformer, the switching frequency should be as high as possible. In this paper, the switching frequency f_s is set to 220 kHz, so the primary inductance L_p is 10 μ H. Due to the high switching frequency, a multilayer ceramic capacitor with a smaller capacitance value can be used as an output filter capacitor instead of a larger electrolytic capacitor to further reduce the size of the power supply. In order to prevent the leakage inductance of the transformer from breaking down the switching tube, a transformer buffer circuit is designed to suppress the leakage inductance peak; and an output diode absorption circuit is designed to suppress the ringing caused by the junction capacitance of the secondary diode and protect the diode. However, APD has high requirements on voltage stability. In Geiger mode, a small change in bias voltage may cause a great change in the gain characteristics of APD. Therefore, adding an LC filter circuit at the output can further reduce ripple wave.

The core control chip of the control circuit uses a current type pulse width modulation (PWM) controlled DC/DC converter chip LT8580, which contains a 1 A and 65 V switch inside. Its switching frequency can be set between 200 kHz and 1.5 MHz by a single resistor, and current can be limited periodically. It is generally used in flyback converters. The chip has complete functions, integrated with undervoltage latch, internal soft

start, overheat start, and other functions. In addition, it has the advantages of small package size, simple peripheral circuit design, and fewer pins.

This paper designs a current-controlled flyback converter structure^[19], as shown in Fig.2. It uses a dual-loop control structure to achieve feedback control, which are the current feedback loop inside the chip and the voltage feedback loop outside the chip. The LT8580 chip integrates a sampling resistor to sample the current passing through the switch tube to form a voltage proportional to the switch current. This voltage is amplified by an internal amplifier, loaded onto a stable ramp, and fed to the non-inverting input of the internal PWM comparator, forming a current feedback loop. The voltage feedback loop uses an external error amplifier to input the voltage error to the VC terminal of the chip, skipping the internal operational amplifier circuit of the chip, so that the dynamic response speed of the power supply is greatly improved. The error amplifier selects AD8628, a precision operational amplifier with high precision and low temperature drift characteristics. With its offset voltage as low as 1 μ V and temperature drift of 2 nV/ $^{\circ}$ C, it can effectively reduce the error and temperature drift of the output voltage.

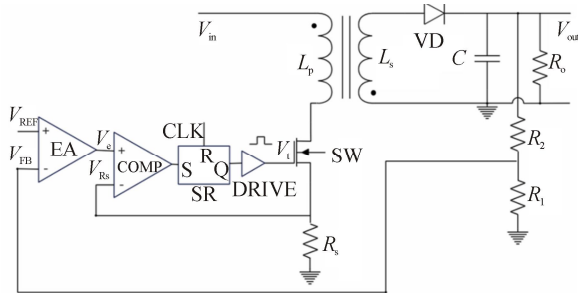


Fig.2 Schematic for the current control mode flyback converter

As shown in Fig.3, the error amplifier is essentially an inverting amplifier. For the amplifier circuit designed in this paper, temperature drift is the main source of the amplification error. In addition to using an operational amplifier with a low drift coefficient, it is also critical to use a resistor with high stability. The APD bias power supply sampling resistor shunt designed in this paper satisfies the following formula

$$I_B = V_{out} / (R_{f1} + R_{f2}), \quad (3)$$

where I_B is the sampling current, R_{f1} and R_{f2} are respectively the upper and lower sampling resistors, and V_{out} is the output voltage. The output voltage of the power supply designed in this paper is as high as several hundred volts, and the APD reverse bias current in Geiger mode is less than 1 mA. At this time, if the sampling resistance is small, the sampling current will greatly affect the power supply efficiency. In order to reduce the shunt effect of the sampling network, the sampling resistor needs to reach mega ohms. In the voltage control loop, the error amplifier amplifies the error between the

sampling voltage and the reference voltage. Combined with the design of the feedback compensation loop, the feedback resistance must be several times the sampling resistance, and a high-impedance resistor above megohm is also required. However, a high-resistance resistor with a resistance value above 1 M Ω has poor stability and may cause large temperature drift, which affects the output accuracy and stability of the power supply. At the same time, high resistance resistors with high precision and low temperature drift are expensive and difficult to select. High-resistance resistors have good insulation and are more susceptible to pollution during soldering processes, such as flux and printed circuit board (PCB) leakage problems, resulting in increased output errors.

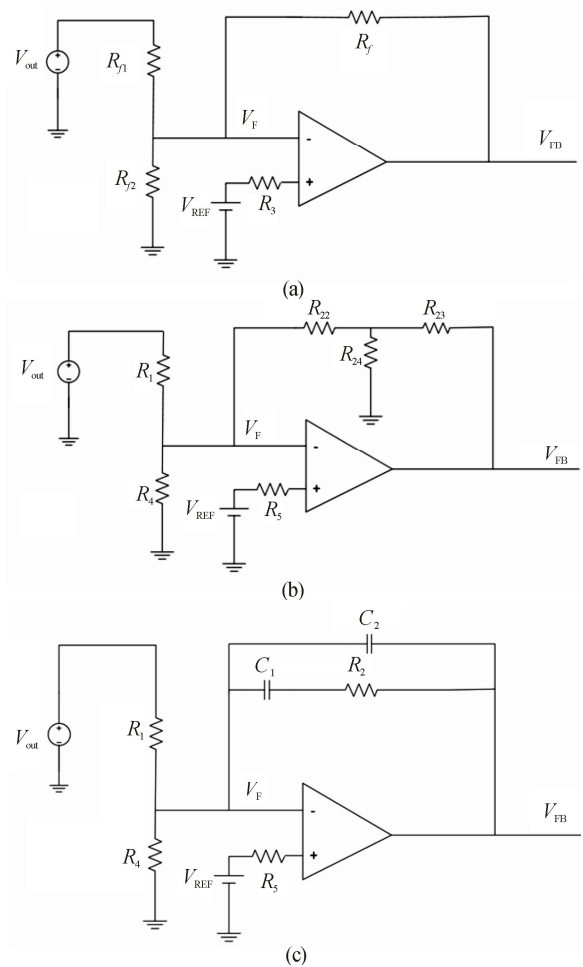


Fig.3 Diagrams of error amplifiers: (a) Traditional DC scheme; (b) T-type resistor feedback DC scheme; (c) Zero-pole compensation network

Aiming at various problems of high-impedance resistors, this paper uses a T-type resistor feedback network to replace the high-impedance resistor in the original amplifier circuit, as shown in Fig.3. The virtual short and virtual break characteristics of the operational amplifier are

$$V_- \approx V_+ = 0, \quad (4)$$

$$I_- \approx 0. \quad (5)$$

According to Kirchhoff's current law, the current on

the resistor satisfies

$$I_{R23} = I_{R22} + I_{R24}, \quad (6)$$

$$I_{R22} = I_{in}. \quad (7)$$

The equivalent feedback resistance can be obtained as

$$R_{f_equ} = R_{22} + R_{23} + \frac{R_{22} \times R_{23}}{R_{24}}. \quad (8)$$

From Eq.(8), it can be seen that through R_{22} , R_{23} , and R_{24} , the three smaller resistors can be used as a large feedback resistor by taking appropriate values. In this paper, R_{22} is 100 k Ω , R_{23} is 10 k Ω , and R_{24} is 200 Ω . The resistance values are all less than 1 M Ω , and the equivalent feedback resistance R_{f_equ} is 5.11 M Ω .

From the above discussion, it can be concluded that the T-type resistor network used in this paper achieves a large comparison coefficient through a small resistor, realizes a high resistance value of the equivalent feedback resistor, and avoids the shortcomings of high-resistance resistors^[20]. At the same time, in terms of circuit design, only two resistors are added compared to the traditional circuit, which does not significantly increase the cost and complexity of the circuit. The T-type resistor feedback network designed in this paper can effectively reduce the temperature drift of the error amplifier circuit, improve the accuracy and stability of the output voltage, and fully meet the high precision and high stability requirements of the APD bias power supply.

After the main circuit is designed according to the characteristics of the APD, it is necessary to design a compensation network to further improve the system performance. Compensating the system first needs to determine the transfer function of the main circuit of the power stage, so as to determine the transfer function of the error amplifier, and calculate the crossover frequency, that is, the frequency at which the gain curve is 0 dB. Through parameter design, the slope of the gain curve at the crossover frequency is 20 dB/dec to realize feedback compensation^[21].

In the compensation design, the compensation network is often designed under the worst working condition, that is, the minimum input voltage and full load working condition, to ensure that the control loop can remain stable under all working conditions. At this time, the DCM mode can be regarded as being in the critical conduction mode (BCM), and the transfer function can be calculated according to the continuous conduction mode (CCM), and the transfer function of the main circuit in the current control mode can be obtained as

$$G(s) = \frac{nRV_{in}}{(2nV_o + V_{in})R_s} \times \frac{(1 + R_{est}C_s)(sL_pD)}{1 + \frac{CR_s}{1+D}}, \quad (9)$$

where R_s is the sampling resistor, and C is the output filter capacitor. From Eq.(9), the transfer function produces a zero point by the equivalent series resistance of the output capacitance R_{est} . The pole is related to the equivalent resistance of the load R . In addition, there is a

right-half-plane zero point, which is not easy to compensate. In order to reduce the interference of right-half-plane zero point, the only way to design parameters is as far away from this zero point as possible.

In this paper, a zero-pole compensator is used as shown in Fig.3(c), and the DC gain from the output terminal of the error amplifier to the output voltage is

$$G_{DC} = \frac{nRV_{in}}{(2nV_o + V_{in})R_s}. \quad (10)$$

The maximum duty cycle D does not exceed 0.5, the turns ratio n is 10, and the sampling resistor R_s is 0.02 Ω . The DC gain of the transmission stage can be obtained as

$$A_{DC} = 20 \lg \left(\frac{nRV_{in}}{(2nV_o + V_{in})R_s} \right) \approx 56.7 \text{ dB}. \quad (11)$$

And the right half plane zero point is

$$f_{RHZ} = \frac{n^2 R(1-D)^2}{2\pi L_p D} \approx 71.6 \text{ kHz}. \quad (12)$$

According to the loop stability criterion, the crossover frequency should be less than 30% of the zero point of the right half plane. At the same time, the crossover frequency should be less than 1/10 of the switch, and the switching frequency is 220 kHz, and the crossover frequency can be obtained as 20 kHz to determine the position of the zero pole of the compensation network:

$$f_{cz} = \frac{f_c}{3} \approx 6 \text{ kHz}, \quad (13)$$

$$f_{cp} = 3f_c = 60 \text{ kHz}. \quad (14)$$

Determine the position of the output filter pole. When other conditions remain unchanged, the output filter pole is proportional to the load, then

$$f_{fp} = \frac{1}{2\pi R_{max} C} \approx 3.5 \text{ Hz}, \quad (15)$$

$$G_{xo} = 20 \lg \left(\frac{f_{xo}}{f_{fp}} \right) - G_{DC} \approx 18.4 \text{ dB}, \quad (16)$$

$$A_{xo} = 10^{\left(\frac{G_{xo}}{20}\right)} \approx 8. \quad (17)$$

According to Eq.(17), it can be obtained that R_2 is about 5 to 10 times of R_1 , and taking the up-sampling resistor R_1 as 1 M Ω , R_2 can be obtained as 5 M Ω . That is to say, the capacitance parameter in the compensation network is

$$C_2 = \frac{1}{2\pi f_{cp} R_2} = 0.5 \text{ pF}, \quad (18)$$

$$C_1 = \frac{1}{2\pi f_{cz} R_2} = 5.3 \text{ pF}. \quad (19)$$

Take C_1 as 0.5 pF, C_2 as 5 pF, and R_2 as 5 M Ω . Then, we use MATLAB to simulate and verify the system transfer function, and the Bode diagram is shown in Fig.4.

It can be seen that when the system is added with compensation, the system responds faster, the phase margin at the crossover frequency is 55°, and the system stability is enhanced. In addition, the attenuation of the

high-frequency band is also very large, which suppresses high-frequency noise, such as switching noise well.

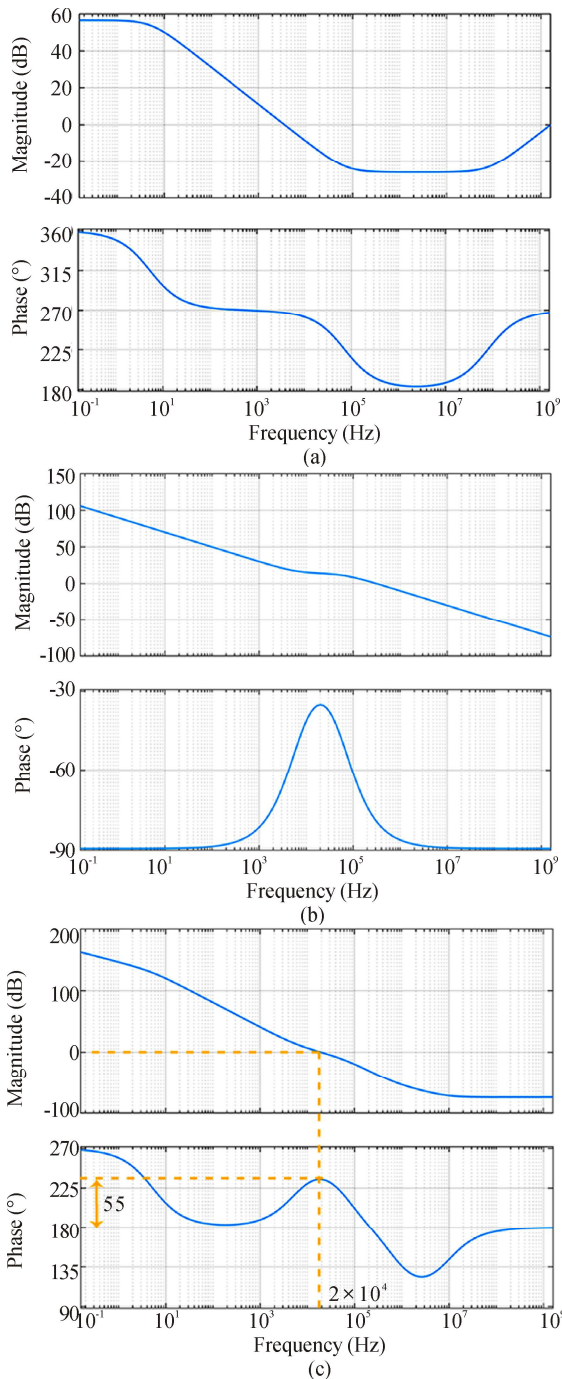


Fig.4 Bode diagrams of (a) the main circuit, (b) the compensating network, and (c) the compensated system

This paper uses the simulation software LTspice to simulate and verify the power system. This software has the advantages of fast simulation speed and friendly user interface. The capture of circuit diagrams and the observation of waveforms can be realized, and models and improvements are provided for simplifying active devices.

As shown in Fig.5, the output voltage rises to 450 V in

about 30 ms, which meets the design requirements. The voltage and current waveforms on the primary and secondary coil of the transformer conform to the basic characteristics of the flyback converter in DCM mode, as shown in Fig.6, which verifies the feasibility of the system.

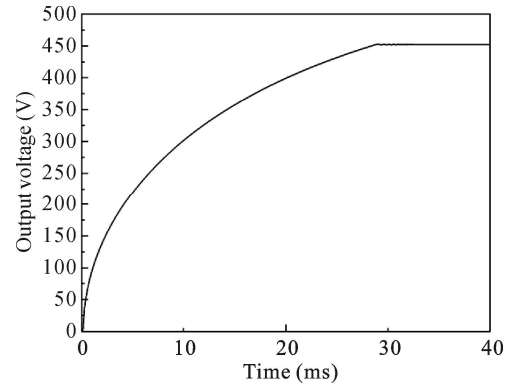


Fig.5 Simulation diagram of the maximum output voltage

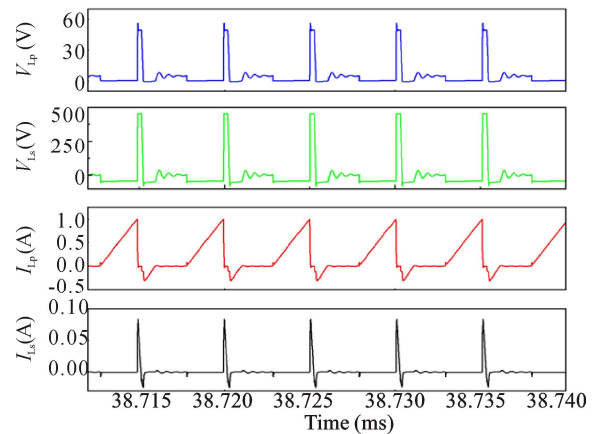


Fig.6 Voltage and current waveform diagrams on the coils L_p and L_s of the transformer

The final experimental prototype is shown in Fig.7, the size of the power supply is 2.5 cm×2.5 cm, the input voltage is 5 V, by adjusting the control voltage, the output voltage can be adjusted between 0—450 V, and the maximum input current does not exceed 0.2 A. The maximum power consumption is about 1 W.

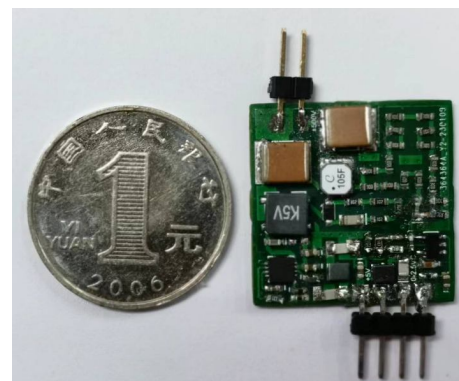


Fig.7 Prototype of the power supply (compared in size with a one-yuan coin)

The APD bias voltage output voltage is 201 times that of the control voltage. We measured the control voltage U_{REF} and output voltage U_O' with multimeter Agilent34410A, calculated the theoretical output voltage U_O , and determined the precision of the output voltage γ_V , as shown in Tab.1.

Tab.1 Analysis of output voltage precision

$U_{REF}(V)$	$U_O(V)$	$U_O'(V)$	γ_V
0.102	20.502	20.493	0.044%
0.202	40.602	40.558	0.108%
0.302	60.702	60.594	0.178%
0.402	80.802	80.645	0.194%
0.502	100.902	100.563	0.336%
0.602	121.002	120.590	0.340%
0.702	141.102	140.606	0.352%
0.802	161.202	160.633	0.353%
0.902	181.302	180.525	0.429%
1.002	201.402	200.546	0.425%
1.102	221.502	220.557	0.427%
1.202	241.602	240.561	0.431%
1.301	261.501	260.561	0.359%
1.402	281.802	280.454	0.478%
1.502	301.902	300.455	0.479%
1.602	322.002	320.457	0.480%
1.702	342.102	340.420	0.492%
1.801	362.001	360.304	0.469%
1.901	382.101	380.292	0.473%
2.002	402.402	400.425	0.491%
2.101	422.301	420.286	0.477%
2.201	442.401	440.254	0.485%
2.251	452.451	450.204	0.497%

In Tab.1 and Fig.8, it can be obtained that the accuracy of the output voltage is better than 0.5% in the range of 0—450 V, and the output voltage and control voltage have good linearity, which meets the design requirements.

The output ripple is tested with an oscilloscope RIGOLDS2072A. When the output voltage is 450 V, the ripple is shown in Fig.9, the ripple is only 5.4 mV, and the power supply ripple ratio is 0.001 2%, which meets the high stability requirements of the APD in Geiger mode.

To sum up, this paper proposes a high-precision, low-ripple, high-stability and small-volume Geiger-mode APD bias power solution. The input voltage is 5 V, and the maximum output voltage can be as high as 450 V, achieving 90 times amplification. The feedback circuit

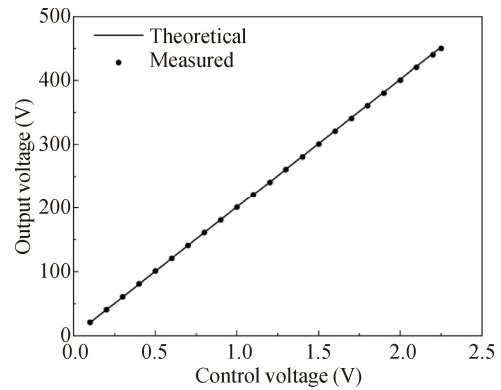


Fig.8 Theoretical output voltage and measured output voltage vs. the control voltage

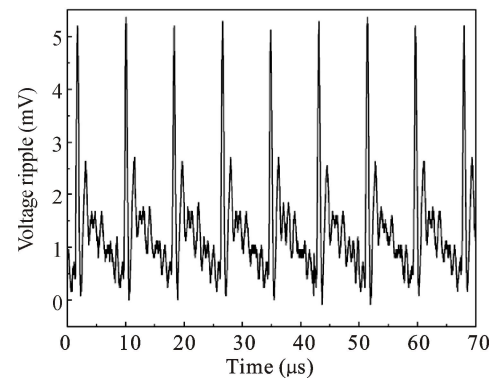


Fig.9 Voltage ripple at 450 V output

uses a high-precision operational amplifier and designs a T-type resistor feedback network, which avoids the instability and high cost of high-value resistors, improves the output voltage accuracy and temperature stability, and the output voltage accuracy is as high as 0.5%, the maximum ripple is 5.4 mV, and the power supply ripple ratio is only 0.001 2%. And a reasonable compensation network is designed to improve the stability and response speed of the power system. In addition, the overall size of the circuit board is controlled to 2.5 cm×2.5 cm, and the maximum power does not exceed 1 W, which can meet the needs of various APD application scenarios and has certain guiding significance for the voltage module design of small detection equipment, such as handheld laser rangefinders and lidar.

Ethics declarations

Conflicts of interest

The authors declare no conflict of interest.

References

[1] GAO B, WU Z H, SHI W X, et al. Ability of strong-pulse illumination to hack self-differencing avalanche photodiode detectors in a high-speed quantum-key-distribution system[J]. Physical review A, 2022, 106(3): 033713.
 [2] GHEZZI A, FARINA A, BASSI A, et al. Multispectral

- compressive fluorescence lifetime imaging microscopy with a SPAD array detector[J]. *Optics letters*, 2021, 46(6): 1353-1356.
- [3] BARTOLO-PEREZ C, CHANDIPARSI S, MAYET A S, et al. Avalanche photodetectors with photon trapping structures for biomedical imaging applications[J]. *Optics express*, 2021, 29(12): 19024-19033.
- [4] ZHOU X, SUN J F, JIANG P, et al. Improvement of detection probability and ranging performance of Gm-APD LiDAR with spatial correlation and adaptive adjustment of the aperture diameter[J]. *Optics and lasers in engineering*, 2021, 138: 106452.
- [5] WIPIEJEWSKI T, AKULOVA Y A, FISH G, et al. Integration of active optical components[J]. *Proceedings of SPIE - the international society for optical engineering*, 2003, 4997: 1-12.
- [6] TALAVÁN D, ESPAÑA S. Dynamic light scattering based on low-cost components[J]. *Measurement science and technology*, 2022, 33(6): 065902.
- [7] RAWAT A, AHAMED A, BARTOLO-PEREZ C, et al. Design and fabrication of high-efficiency, low-power, and low-leakage Si-avalanche photodiodes for low-light sensing[J]. *ACS photonics*, 2023, 10(5): 1416-1423.
- [8] CHEN Q S, ZHANG M. Technology and application of silicon avalanche photodiode[J]. *Electronics & packaging*, 2021, 21(3): 030101. (in Chinese)
- [9] BARTOLONI A, BARONE L M, CAVALLARI F, et al. High voltage system for the CMS electromagnetic calorimeter[J]. *Nuclear instruments and methods in physics research section A: accelerators, spectrometers, detectors and associated equipment*, 2007, 582(2): 462-468.
- [10] WEI Z J, WANG J D. A high precision avalanche photon diode bias power supply[J]. *Telecom power technology*, 2011, 28(04): 73-74. (in Chinese)
- [11] YANG Y Y, WANG S W, HSIEH C Y, et al. Power management with a low-ripple high-conversion-ratio 80-V output voltage boost converter for avalanche photodiode system[J]. *IEEE transactions on industrial electronics*, 2013, 60(7): 2627-2637.
- [12] XING H C, XU J T, LI X Y, et al. Development of Geiger mode circuit with silicon avalanche photodiode for ultraviolet optical communication[J]. *Infrared technology*, 2018, 40(10): 966-971. (in Chinese)
- [13] XIANG Y Y, GUO S G, WU Y, et al. Design of an APD bias voltage module with high precision and low power consumption[J]. *Semiconductor optoelectronics*, 2021, 42(04): 556-561+567. (in Chinese)
- [14] YAU Y T, HUNG T L. A flyback converter with novel active dissipative snubber[J]. *IEEE access*, 2022, 10: 108145-108158.
- [15] PATRA S, SAHU S K, ABICHANDANI P G, et al. Self-operating flyback converter for boosting ultra-low voltage of thermoelectric power generator for IoT applications[J]. *IEEE transactions on industrial electronics*, 2022, 69(12): 12957-12966.
- [16] LIANG T J, CHEN K H, CHEN J F. Primary side control for flyback converter operating in DCM and CCM[J]. *IEEE transactions on power electronics*, 2018, 33(4): 3604-3612.
- [17] LUO H, ZANG T L, CHEN S, et al. An adaptive off-time controlled DCM flyback PFC converter with unity power factor and high efficiency[J]. *IEEE access*, 2021, 9: 22493-22502.
- [18] HOWIMANPORN S, BUNLAKSANANUSORN C. Performance comparison of continuous conduction mode (CCM) and discontinuous conduction mode (DCM) flyback converters[C]//The Fifth International Conference on Power Electronics and Drive Systems, November 17-20, 2003, Singapore. New York: IEEE, 2003, 2: 1434-1438.
- [19] HIMANSHU, KHANNA R. Various control methods for DC-DC buck converter[C]//2012 IEEE Fifth Power India Conference, December 19-22, 2012, Murthal, India. New York: IEEE, 2012: 1-4.
- [20] YU X Y, CHEN H F, ZOU H, et al. Simulation of a preamplifier for an extremely weak current measure circuit[J]. *Nuclear electronics & detection technology*, 2014, 34(12): 1514-1517. (in Chinese)
- [21] SANJAYA M. *Switching power supplies A to Z*[M]. WANG Z Q, ZHU W, LI Y Y, et al, Transl. 2nd ed. Beijing: Posts & Telecom Press, 2015: 328-351.